Rats spontaneously perceive global motion direction of drifting plaids

Giulio Matteucci[1,2,*], Benedetta Zattera[1,3,*], Rosilari Bellacosa Marotti[1], and Davide Zoccolan[1,#]

1. Visual Neuroscience Lab, International School for Advanced Studies (SISSA), Trieste, 34136, Italy

2. Current address: Department of Basic Neurosciences, University of Geneva, Geneva, 1206, Switzerland

3. Current address: Friedrich Miescher Institute for Biomedical Research (FMI), Basel, 4058, Switzerland

**These authors contributed equally to this work*

Corresponding author

Davide Zoccolan
International School for Advanced Studies (SISSA)
Via Bonomea, 265 34136 Trieste (TS) ITALY
Office: +39 040 3787 701 Fax: +39 040 3787 702
E-mail: zoccolan@sissa.it

Summary

Computing global motion direction of extended visual objects is a hallmark of primate high-level vision. Although neurons selective for global motion have also been found in mouse visual cortex, we still do not know whether rodents can combine multiple motion signals into global, integrated percepts. Here, we trained two groups of rats to discriminate motion direction of either gratings or plaids (i.e., superpositions of two gratings) and we tested whether these visual patterns were able to prime rat perception consistently with an integrated representation of plaid direction. We found that, depending on the identity of the training stimuli, rats displayed either a shared representation of gratings and plaids based on global motion, or a non-shared one. As shown by computational modeling, these findings are consistent with the existence of a population of pattern-like cells, playing a functional role similar to that demonstrated in primates.

Introduction

Extracting global motion direction of visual objects is crucial to guide behavior in many ethological contexts (Lisberger, 2015; Nishida et al., 2018). Such computation has been widely studied in the dorsal stream of primates, and, in particular, in the middle temporal area (MT) of the macaque (Born and Bradley, 2005). This area is known to receive direct input from neurons in primary visual cortex (V1), which signal the "local" direction of moving elements (e.g., edges) in their small, localized, receptive fields (RF). MT units appear to combine the afferent V1 inputs in such a way to acquire selectivity for the "global" motion direction of visual objects (or patterns) made of multiple local edges (Orban, 2008). The leading hypothesis emerging from the primate literature is that this is achieved by integrating the local motion signals carried by V1 afferents over different spatial positions, directions and frequencies (Adelson and Movshon, 1982; Born and Bradley, 2005; Orban, 2008). Such integration is necessary, because the local output of any V1-like edge detector is intrinsically ambiguous insofar global motion is concerned. Any local output can be generated by infinite combinations of global object directions and speeds. This ambiguity is at the core of what is known, in the psychophysics literature, as the "aperture problem" (Fennema and Thompson, 1979; Wuerger et al., 1996; Marr, 2010): only by combining information from multiple, local, moving-edge detectors, it is possible to infer global motion direction. Achieving a circuit level understanding of such computation remains a key question in visual neuroscience.

Over the past 10 years, the development of a wide array of tools for the dissection of neural circuits (Luo et al., 2008, 2018; Fenno et al., 2011; Chen et al., 2013; Madisen et al., 2015), combined with the demonstration of advanced visual behaviors in mice and rats (Carandini and Churchland, 2013; Zoccolan, 2015), has fostered the use of rodents as model systems to study visual cortical processing. This led some investigators to look for the signature of motion integration in the rodent brain (Juavinett and Callaway, 2015; Muir et al., 2015; Palagina et al., 2017). Inspired by monkey studies (Simoncelli and Heeger, 1998; Smith et al., 2005; Rust et al., 2006; Solomon et al., 2011), they recorded the responses of mouse visual cortical neurons to drifting gratings and coherent plaids − i.e., complex visual patterns made of two overlapping gratings with the same contrast and speed, but moving along independent directions. These stimuli have been widely used to investigate motion integration in human and non-human primates since they enable to clearly distinguish local- from global-based motion responses. A plaid, in fact, has two well-defined local motion components and a global direction that is different from the local ones, while, for a grating,

the local and global directions coincide (Adelson and Movshon, 1982). By employing these stimuli, mouse visual neurons were classified as “pattern” (i.e., responsive to global motion) or “component” (i.e., responsive to local motion). The majority of neurons amenable to such classification fell into the component category, but a small fraction of pattern units was reported in V1 (Muir et al., 2015; Palagina et al., 2017) and in two extrastriate areas, the lateromedial (LM) and rostrolateral (RL) areas (Juavinett and Callaway, 2015). However, the relevance of such tiny population of pattern cells in determining mouse motion perception was left untested [but see further discussion of (Palagina et al., 2017) below].

Even if a few studies tested the ability of rats and mice to discriminate the dominant motion direction of random dot kinematograms (Douglas et al., 2006; Stirman et al., 2016; Marques et al., 2018; Samonds et al., 2018) (RDKs: a task linked to motion integration, since it requires spatial pooling of local motion cues), no study ever probed the ability of rodents to integrate into a global motion percept multiple oriented elements moving along different directions. In addition, all the studies employing RDKs explicitly trained the animals in the direction discrimination task. Critically, this prevented assessing the spontaneous, purely perceptual motion integration abilities of naïve rodents. In fact, if feedback (e.g., reward) is provided to an animal about the outcome of his perceptual choices, it may learn to associate a given stimulus to a given response category without necessarily perceiving the sensory quality that the investigator intends to associate to that category (Tafazoli et al., 2012; Zoccolan, 2015; Zoccolan and Di Filippo, 2018). It would thus be impossible to infer from such kind of experiments whether the choices of the animal are driven by a general-purpose representation of global motion direction at the level of visual cortex (as the one found in monkey MT), or by the ability to learn abstract representations of arbitrary stimulus categories in higher-order association areas involved in perceptual decision making, such as posterior parietal cortex (PPC) (Raposo et al., 2014; Licata et al., 2017; Nikbakht et al., 2018; Odoemene et al., 2018).

Only in (Palagina et al., 2017) this confound was avoided, by monitoring the direction of the optokinetic nystagmus (OKN) while presenting plaids to naïve mice. The resulting bimodal distribution of OKN movements tracking both the local-components and the overall global directions of the stimulus is suggestive of mouse ability to spontaneously perceive global motion. However, this conclusion is affected by the intrinsic limitation of OKN-based experiments to probe cortical processing. In fact, OKN is a reflexive phenomenon that is known to be largely controlled by subcortical structures (Smith and Harris, 1991; Harvey et

al., 1997; Stahl, 2004), while motion perception in direction discrimination tasks has been shown to rely heavily on visual cortex (Newsome and Pare, 1988; Salzman et al., 1990; Marques et al., 2018). As a result, it remains unclear whether rodents spontaneously combine independent motion signals (as those found in plaids) into integrated percepts of global motion direction.

Our study was designed to address this question and provide a thorough psychophysical assessment of rat ability to spontaneously perceive the global direction of drifting plaids. To this aim, we relied on a visual priming paradigm (Tafazoli et al., 2012; Zoccolan and Di Filippo, 2018) that allowed measuring the perceptual similarity between gratings and plaids with the same global direction, without explicitly training the animals to associate these stimuli to the same response category.

Results

A visual priming paradigm to probe spontaneous perception of global motion direction

In the first phase of the study (the *training phase*), a group of 11 male Long-Evans rats (referred to as the G group in what follows) was trained to discriminate leftward- from rightward-drifting gratings (Figure 1A, left), using the high-throughput behavioral rig described in (Zoccolan, 2015) and previously employed in several investigations of rat object recognition (Zoccolan et al., 2009; Tafazoli et al., 2012; Alemi-Neissi et al., 2013; Rosselli et al., 2015; Djurdjevic et al., 2018). Another group of 10 rats (referred to as the P group in what follows) was trained to discriminate leftward- from rightward-drifting plaids with a *cross-angle* of 120º – i.e. composite patterns made of the superposition of two gratings drifting along directions that were 120º apart (Figure 1B, left). Rats that maintained at least a criterion performance of 75% correct choices over a four consecutive day period were moved to the second phase of the study to be tested with the priming paradigm (all rats starting the training phase managed to reach such criterion).

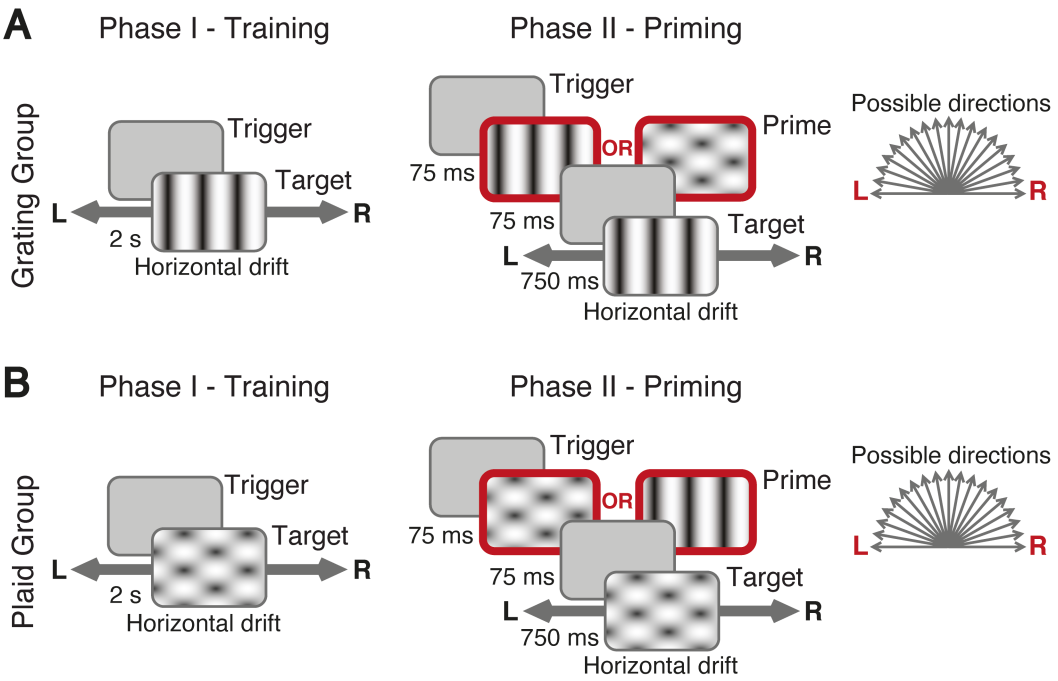

Figure 1. Visual stimuli and discrimination tasks. (**A**) Discriminations tasks administered to the rats of the *grating* (G) *group*. During both the training (left) and priming (right) phases, a trial started when an animal triggered the central port of a 3-way licking sensor (see Materials and methods). During the training phase, a target grating (drifting either leftward or rightward) was presented immediately at the onset of each trial. To receive the reward, a rat had to lick the lateral port corresponding to the direction of motion of the presented target. During the priming phase, the structure of the task was similar, but at the onset of each trial, a drifting prime stimulus was presented for 75 ms, followed by a 75 ms blank screen and finally by the presentation of the target grating (lasting 750 ms). The prime stimulus could move in 19 possible directions (from 0° = right to 180° = left) and could be either a grating or a plaid. (**B**) Discriminations tasks administered to the rats of the *plaid* (P) *group*. The structure of the task was the same as in A, with the key difference that the target stimulus was a plaid instead of a grating (again drifting either leftward or rightward). In this case, the reward was delivered when a rat licked the lateral port corresponding to the global motion direction of the plaid.

In the priming paradigm, the "target" stimulus remained the same as in the training phase (i.e., G and P rats still had to report the direction of drifting gratings and plaids, respectively), but now the presentation of the target was preceded by the brief presentation (75 ms) of either a grating or a plaid drifting along one of 19 possible directions (from 0° = rightward to 180° = leftward, in steps of 10°; Figure 1 A-B, right). The identity (i.e., either grating or plaid) and the motion direction of such "prime" stimulus was randomly selected in each trial. In what follows, we refer to trials in which the identities of prime and target coincide as *identity-priming* condition (e.g., a grating prime stimulus followed by a grating target stimulus), whereas we refer to the opposite case as *cross-priming* condition (e.g., a plaid prime stimulus followed by a grating target stimulus). Critically, the rats kept receiving feedback (i.e., either reward or a time-out period in case of correct and incorrect choices,

respectively) only about the correctness of their responses to the target stimuli. The identity and direction of the prime stimuli were never paired to either the leftward or rightward response categories. As such, the extent to which the prime stimuli were able to affect the choices of the rats was purely due to the spontaneous, perceived similarity between primes and targets. Assessing such similarity was the ultimate goal of our experiments, since it allowed understanding whether, in the cross-priming condition, the perceived motion direction of the plaids was the global one. Based on previous motion adaptation studies in humans (Kanai and Verstraten, 2005) and on former priming/masking experiments carried out in rats (Tafazoli et al., 2012; Alwis et al., 2016; Dell et al., 2018, 2019), we choose the duration of the prime and of the inter-stimulus interval (ISI) between prime and target (75 ms each) in the attempt of inducing a strong priming effect – i.e., in the attempt of biasing rats' responses to the target towards the motion direction of the prime.

In what follows, we will report the accuracy of rats at discriminating the motion direction of a target stimulus as a function of its angular distance from the direction of the prime stimulus that preceded it. As such, the resulting *priming curve* will range between two extremes: 1) the case in which the direction of the prime and target stimuli was the same (e.g., both drifting rightward), referred to as *coherent prime* condition; and 2) the case in which the prime and target stimuli had opposite directions (e.g., the prime drifting rightward and the target drifting leftward), referred to as *incoherent prime* condition. The case in which the prime stimulus drifted vertically (midpoint of the priming curve) will be referred to as *neutral prime* condition. This terminology will be used for both the identity- and cross-priming conditions and for both the P and G groups.

The first step in our analysis was to verify whether the prime stimuli were indeed capable of biasing rat choices depending on the level of coherence between their direction and that of the target stimuli, in case of the identity-priming condition. This was the case for 10 out of 11 rats of the G group and 9 out of 10 rats of the P group, which were therefore included in the subsequent analysis (see Materials and Methods). For the G group, rat group average accuracy at discriminating the motion direction of the target gratings was strongly modulated, as function of the direction of the prime grating stimulus (Figure 2A, black curve). In the coherent prime condition, rat classification of target direction was facilitated, as compared to the reference neutral prime condition (dashed line). Conversely, in the incoherent prime condition, rat classification accuracy was substantially lowered. Overall, the identity-priming curve was approximately sigmoidal. Even for the P group, in the identity-

priming condition, a strong priming was observed (Figure 2B, black curve). Also in this case, the magnitude and sign of the priming effect depended on the similarity between the directions of the prime and target plaid stimuli, resulting in an approximately monotonic drop of rat classification accuracy from the coherent priming condition towards the incoherent one.

The strong modulation of rat classification accuracy in the identity-priming condition has two important implications. First, it demonstrates the effectiveness of the priming paradigm in capturing the perceived similarity between the learned (horizontal) motion directions of the target stimuli and the untrained (previously unseen) directions of the prime stimuli, in the case in which targets and primes are either both gratings or both plaids (i.e. *identity-priming* condition). Second, and more importantly, it serves as a reference against which to compare the modulation of the accuracy observed in the cross-priming condition. In fact, the degree of similarity between the priming curves measured in the identity- and cross-priming conditions (i.e., between the black and gray curves in Figure 2) allows answering two key questions about the neuronal representations of the grating and plaid stimuli.

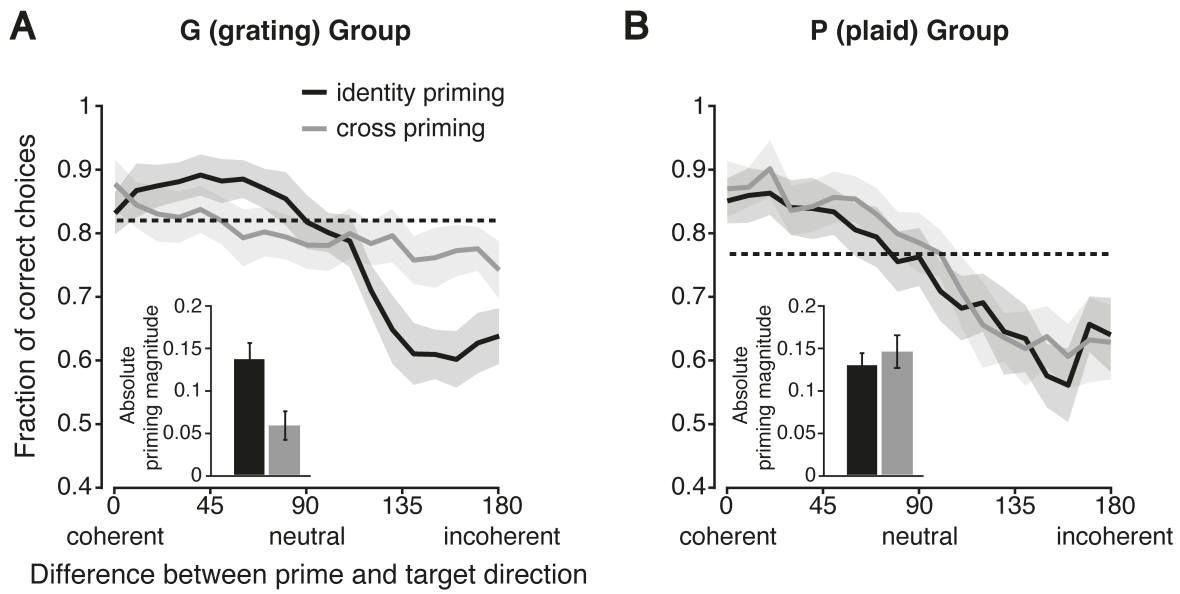

Figure 2. Identity- and cross-priming curves. (**A**) The identity-priming curve (black) reports the mean accuracy of the rats of the G group at discriminating the leftward from the rightward drifting gratings, as a function of the difference between the direction of these target stimuli and the gratings that were used as prime stimuli. The cross-priming curve (gray) reports rat mean accuracy when the plaids were used instead as prime stimuli. The shaded areas are 95% confidence intervals obtained by bootstrap (see Materials and methods). The dashed line shows the accuracy achieved with the neutral identity-prime stimulus (i.e., the grating drifting upward). The inset quantifies the absolute magnitude of priming obtained in the two cases, as the mean absolute difference between the four leftmost (and rightmost) points in a curve and the point corresponding to the neutral condition. The error bars show

95% confidence intervals obtained by bootstrap (see Materials and methods). (**B**) Same as in A, but for the rats of the P group. That is, in this case, the curves report rat mean accuracy at discriminating the leftward from the rightward drifting plaids. The identity-priming curve (black) refers to trials where the plaids were used as prime stimuli, while the cross-priming curve (gray) refers to trials where the gratings were used as primes.

Evidence of a shared representation of gratings' and plaids' motion direction

The first question is whether these representations are "shared" (i.e., the same neural population encodes both gratings and plaids) or "non-shared" (i.e., independent, non-overlapping populations represent the two types of stimuli). In the former case, we would expect a substantial modulation of rat classification accuracy also in the cross-priming condition, possibly as large as in the identity-priming condition. In the latter case, no cross-priming effect would be observable, given the independence of the two populations underlying the perception of gratings and plaids. In case of shared representations, then a second crucial question could be answered by comparing the shapes of the priming curves obtained in the identity- and cross-priming conditions. If rats spontaneously represented the stimuli according to their global direction, then the priming curves produced by gratings and plaids would be very similar, given that, by construction, the global direction of the prime stimuli was the same for matching grating and plaid primes. If the opposite were true, then the priming curves produced by gratings and plaids would be different.

In the G group (Figure 2A), the cross-priming curve (gray) was almost flat and significantly different from the identity-priming curve (black), as shown by the non-overlapping 95% confidence intervals (shaded areas). The priming magnitude produced by the plaid stimuli was found to be significantly smaller than that produced by the gratings (Figure 2A, inset: gray vs. black bar; non-overlapping 95% confidence intervals). This inability of the plaids (when used as prime stimuli) to affect the discrimination (hence the perception) of the target gratings strongly suggests that, for the rats of the G group, the neuronal population representing the direction of the gratings was largely inactive during the presentation of the plaids.

By contrast, in the P group, the cross-priming and identity-priming curves largely overlapped (Figure 2B: gray vs. black curve). As a result, the priming magnitude observed in the two conditions was equally large (Figure 2B, inset: gray vs. black bar; overlapping 95% confidence intervals). In other words, the gratings and plaids (when used as prime stimuli) were equally effective at biasing rat discrimination of the target plaids. This indicates that the

same neuronal population was active during the presentation of both kinds of stimuli, as expected in case of a shared representation of gratings and plaids. More importantly, the priming produced by gratings and plaids was not only equivalent in terms of overall magnitude, but it was also very similar for matching (global) directions of the two stimuli (i.e., overlapping curves in Figure 2B). This strongly suggests that the representation of plaids in rats trained to discriminate such stimuli (P group) is not only shared with the representation of gratings, but is structured in such a way to encode plaids' global motion direction.

Rat perception of drifting plaids is more consistent with a pattern- than a component-based representation of motion signals

To test more formally the extent to which the priming curves observed for the P group are consistent with a representation of global motion direction of the plaid stimuli, we performed a decoding analysis using linear classifiers. We simulated two alternative scenarios: a representation made of pattern cells (i.e., neurons tuned to the global direction of the plaids) and a representation made of component cells (i.e., neurons tuned to the local direction of the constituent gratings of the plaids).

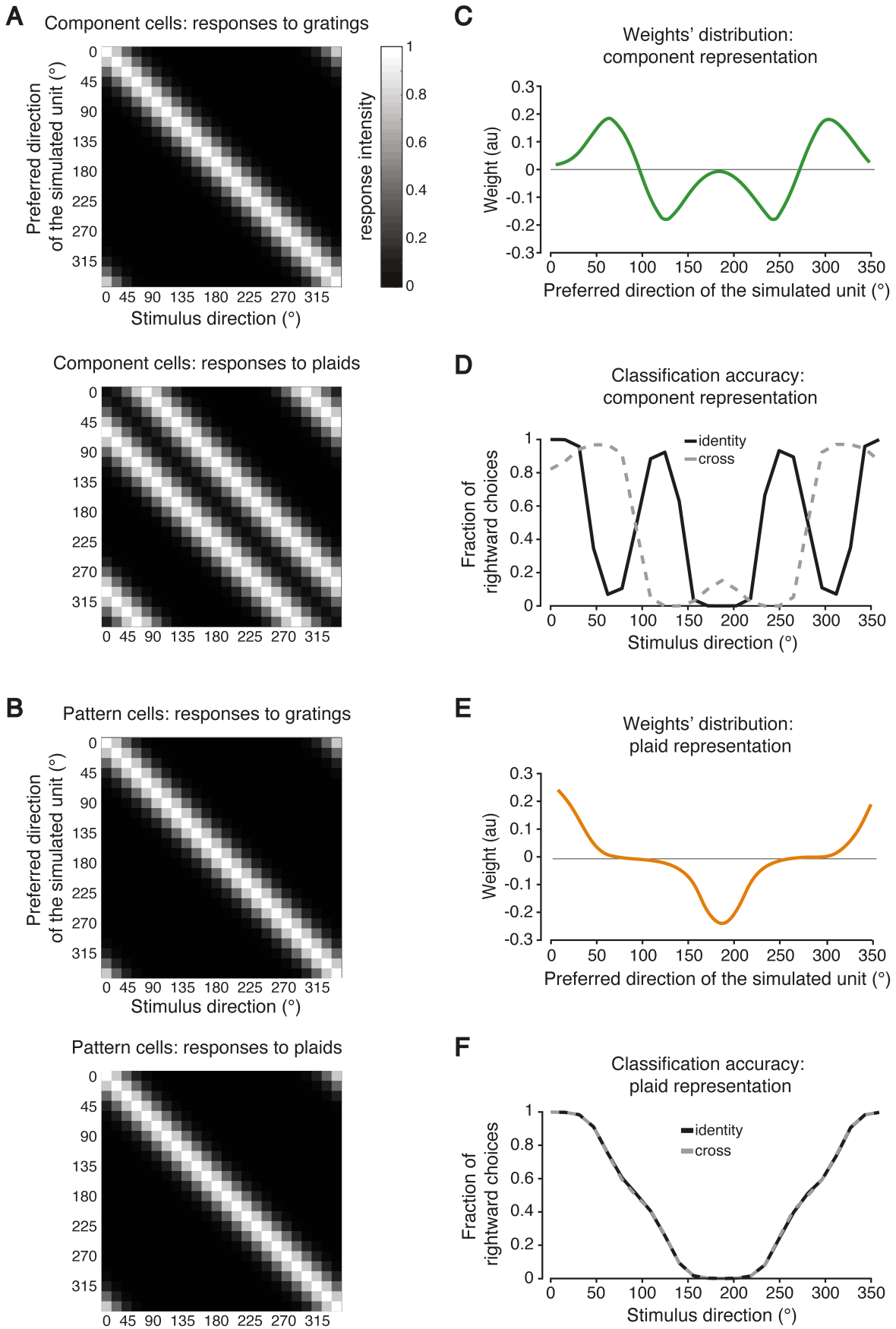
A
Component cells: responses to gratings
Preferred direction of the simulated unit (°)
Stimulus direction (°)
response intensity
Component cells: responses to plaids
B
Pattern cells: responses to gratings
Pattern cells: responses to plaids
C
Weights' distribution: component representation
Weight (au)
Preferred direction of the simulated unit (°)
D
Classification accuracy: component representation
Fraction of rightward choices
identity
cross
Stimulus direction (°)
E
Weights' distribution: plaid representation
F
Classification accuracy: plaid representation

262

Figure 3. Simulating the discrimination accuracy afforded by component- and a pattern-based representations. (**A**) Tuning curves (rows) for a simulated population of 24 components cells, whose preferred directions homogeneously spanned the [0º 360º] range, starting from 0º (first row), up to 345º (last row), in steps of 15º. The responses of the units are shown as a function of 24 possible directions (columns) of the grating (top) and plaid (bottom) stimuli. The gray scale bar indicates the intensity of the response. (**B**) Same as in A but for a population of 24 simulated pattern cells. (**C**) Weights assigned to each of the 24 component cells in A (the x axis reports the preferred direction of each unit) by a logistic classifier that was trained to discriminate a 0º- (rightward) from a 180º-drifting (leftward) plaid. (**D**) Fraction of times that the logistic classifier fed with the component-based representation (whose weights are shown in C) classified the test stimuli as drifting rightward (i.e., at 0º). The test stimuli were either plaids (solid black curve) or gratings (dashed gray curve) spanning the whole [0º 360º] range of directions. (**E**) Weights assigned to each of the 24 pattern cells in B by a logistic classifier that was trained to discriminate a 0º- (rightward) from a 180º-drifting (leftward) plaid. (**F**) Same as in D, but for the logistic classifier fed with the pattern-based representation (whose weights are shown in E). Figure 3–figure supplement 1 reports an extended version of these simulations, where a range of widths of the tuning curves (from very broad to very narrow) was tested.

In both cases, we simulated a population of 24 units, whose preferred directions homogeneously spanned the [0º 360º] range (i.e., one unit tuned to every direction in steps of 15º; Figure 3A-B). The tuning curves of the simulated units were defined by Von Mises functions (Kohn and Movshon, 2004; Matteucci et al., 2019), which are the circular analog of Gaussian functions and whose width is controlled by the parameter k, which is equivalent to the inverse of the variance of a Gaussian distribution (Berens, 2009) (see Methods for details). In our simulations, k was set to 7, which roughly corresponds to a peak of the tuning curve with a full width at half maximum (FWHM) of about 50º (see grayscale matrix in Figure 3A-B). By construction, for a component cell, the response to the drifting plaids as a function of their direction featured two peaks, separated by 120º (Figure 3A, bottom). These peaks correspond to the global directions of the plaid that bring one of the constituent gratings to be aligned to the preferred (local) direction of the unit (i.e., the one shown in Figure 3A, top). Conversely, the tuning curves of the simulated pattern cells featured a single peak, corresponding the global direction of the stimulus (no matter whether grating or plaid) they were tuned to (Figure 3B) (see Methods for further details).

We used these populations to simulate how a rat trained to discriminate leftward from rightward drifting plaids (i.e., same task of the animals in the P group; see Figure 1B) would spontaneously categorize the novel, previously unseen gratings and plaids used as prime

stimuli, under the assumption of either a purely pattern-based or a purely component-based representation. Rat perceptual decisions were simulated by training a logistic classifier to discriminate the leftward from the rightward drifting plaids, based on their representation in the simulated neural population space. As a result of the training, each classifier learned to rely on a specific subset of the units of the representation, as shown by the weights' distribution of Figure 3C and E. We then tested how each classifier categorized the sets of drifting plaids and gratings used in the identity- and cross-priming experiments. This yielded generalization curves (Figure 3D and F) that, in the [0º 180º] range, are equivalent to the identity- and cross-priming curves of Figure 2B.

The shape of the generalization curves can be understood by considering the corresponding weights' distribution resulting from training with the 0º- and 180º-drifting plaids. In the case of the component representation, these training stimuli activated mostly the units tuned for directions at ±60º with respect to the direction of the stimuli themselves. As a result, the classifier learned to assign large, positive weights to the units tuned at ~60º and ~300º (i.e., those providing the strongest evidence of a rightward, 0º-drifting plaid), and large, negative weights to the units tuned at ~120º and ~240º (i.e., those providing the strongest evidence of a leftward, 180º-drifting plaid) – hence, the twin positive and negative peaks in the weights' distribution (Figure 3C).

When the classifier was presented with test plaids spanning the whole [0º 360º] range of directions, the proportion of rightward choices (solid curve in Figure 3D) was obviously maximal (i.e., 100%) at 0º (since this was the rightward training direction), but then dropped quickly, becoming minimal (i.e., 0%) for a plaid drifting at 60º. In fact, for this stimulus, one of the constituent gratings activated the units tuned at ~0º, where the weights were close to zero (see Figure 3C), while the other grating activated the units tuned at ~120º, where the weights were large but negative, since those units signaled the presence of the leftward, 180º-drifting plaid. When the direction of the test plaid further increased, the proportion of rightward choices grew again, reaching a new positive peak at 120º. This was because one of the constituent gratings of the plaid activated the units tuned at 60º (with large, positive weights), while the other grating activated those tuned at 180º (where the weights were close to zero). The generalization curve reached again another minimum when the test plaid drifted at 180º (the leftward training direction), with the constituent gratings that activated the units tuned at 120º and 240º, with large, negative weights. As shown in Figure 3D, a mirror trend was produced for plaids drifting along directions larger than 180º.

As for the generalization curve obtained when feeding to the classifier isolated drifting gratings (dashed, gray curve in Figure 3D, which is equivalent to the cross-priming curve of Figure 2B), it largely followed the shape of the weights' distribution. This can be easily understood, given that a grating provided as much evidence of rightward (leftward) motion as close its direction was to the positive (negative) peaks of the weights' distribution. As a result, the generalization curves produced by plaids and gratings (solid vs. dashed curve in Figure 3D) followed completely different trends, with no overlap. In addition, none of them matched the monotonic decrease observed for the corresponding identity- and cross-priming curves of Figure 2B (solid vs. dashed curve). Together, this strongly suggests that a representation made of component cells is incompatible with the priming curves measured for the rats of the P group.

A very different result was found for the simulated representation of pattern cells. In this case, the weights' distribution had a large, positive peak at 0º, corresponding to the units coding for the rightward motion, as well as a large, negative peak at 180º, corresponding to the units coding for the leftward motion (Figure 3E). Given that, by construction, the pattern cells responded in the same way to isolated gratings and plaids having the same (global) direction, the generalization curves corresponding to the identity- and cross-priming conditions fully overlapped (Figure 3F, black, solid line vs. gray, dashed line). More importantly, they both followed a monotonic, decreasing trend in the [0º 180º] range, which largely trailed the shape of the weights' distribution. Crucially, these trends were highly consistent with those observed for the priming curves of Figure 2B. This shows that, differently from the case of the component representation, a representation made of pattern cells would support the identity- and cross-priming curves obtained for the rats of the P group.

To verify the extent to which this conclusion depended on the width of the tuning curves of the simulated units, we allowed the parameter k (that defines the width of the Von Mises functions) to range from 0.5 to 11. Examples of the resulting tuning curves obtained for the simulated component cells are shown in Figure 3–figure supplement 1A. At very low k, as a result of the increased broadness of the tuning, the two peaks in the response to the plaid stimuli (solid curves) tended to merge. This translated in a broadening of the weights' distribution of the logistic classifier (Figure 3–figure supplement 1B) and in a concomitant increase of the similarity between the generalization curves obtained for gratings and plaids (Figure 3–figure supplement 1C; dashed vs. solid curves). To quantify this similarity, we

computed the absolute differences between the proportions of rightward choices in the two generalization curves across all tested directions and we averaged them. The resulting average difference was large (as already shown in Figure 3D) for $k > 5$ but became negligible for $k < 3$ (Figure 3–figure supplement 1D). This corresponds to peaks in the tuning curves with FWHM ~ 80° or wider (see Figure 3–figure supplement 1A). Therefore, a population of component cells with such a broad tuning could in principle account for the overlapping identity- and cross-priming curves obtained for the P group in our experiments (Figure 2B).

To understand whether this is a plausible scenario, one would need to measure the width of tuning of component cells in rodent visual cortex. Unfortunately, the few studies investigating component and pattern cells in mouse visual cortex did not perform a statistical characterization of the sharpness of their orientation tuning. This prevented our simulated units from quantitatively matching a physiological ground-truth in terms of orientation tuning. Nevertheless, the tuning curves of the example component cells reported in rodent studies investigating this topic feature such sharp and narrow peaks over the orientation axis to decisively fall in the regime corresponding to $k >> 5$ in our simulations (i.e., with FWHM << 60°) (Juavinett and Callaway, 2015; Palagina et al., 2017). A similar conclusion is supported by the general tendency of orientation tuning to be quite sharp in mouse and rat visual cortex (Girman et al., 1999; Niell and Stryker, 2008; Gao et al., 2010; Marshel et al., 2011; Vermaercke et al., 2014; Ghodrati et al., 2016; Matteucci et al., 2019; Matteucci and Zoccolan, 2020). As such, the most likely hypothesis is that the stimulus representation underlying the priming curves of the P group (Figure 2B) consisted of pattern, rather than component cells. Further neurophysiological studies will be necessary to verify this hypothesis – e.g., by directly testing, as done here in our simulations, the extent to which populations of recorded component and pattern cells yield direction classification curves that are consistent with the priming curves measured in our experiments.

Discussion

The results presented in Figure 2B show that rats are capable of spontaneously combining local motion cues into integrated percepts of global motion direction of a complex visual pattern. Our simulations show that this ability is consistent with a representation of global motion signals, as the one provided by pattern cells (Figure 3 and Figure 3–figure supplement 1). As such, our findings strongly suggest that rats are capable of processing motion stimuli

396 by relying on pattern-like representations. This, in turn, establishes a candidate perceptual
397 correlate of the neuronal selectivity for global motion previously reported across rodent
398 visual cortical areas (Juavinett and Callaway, 2015; Muir et al., 2015; Palagina et al., 2017),
399 suggesting that, despite being a tiny fraction of the overall visual cortical population, rodent
400 pattern cells do play an important (possibly preferential) role in the processing of visual
401 motion. Critically, such motion integration ability only emerged in rats trained to discriminate
402 the plaid stimuli (P group). The animals trained in the grating discrimination task (G group)
403 were instead virtually insensitive to the plaids (Figure 2A), indicating that the neuronal
404 population they relied upon to encode the gratings failed to effectively represent the plaids. In
405 the following sections we provide two tentative explanations of such observations based on
406 different sets of assumptions. Simulations of component- and pattern-based representations
407 and linear read-out mechanisms (similar to those shown in Figure 3) allowed testing the
408 ability of such assumptions to possibly explain our findings.

409 **Simulating a scenario where training with either gratings or plaids leads to a decoding**
410 **pool enriched of either component or pattern cells.**

411 The first explanation rests on the hypothesis that the specific discrimination being
412 reinforced during the training biased the recruitment of the visual cortical pool that was read
413 out by downstream decision neurons towards either a more component-enriched or a more
414 pattern-enriched cell population (referred to as the "decoding pool" in what follows). Such a
415 task-dependent selection of the decoding pool may stem from differences between
416 component and pattern cells in terms of two key properties: i) their relative proportion within
417 visual cortex; and ii) the intensity of their responses to gratings and plaids.

418 With regard to the first property, although the number of studies investigating motion
419 integration in rodent visual cortical areas is still limited (Juavinett and Callaway, 2015; Muir
420 et al., 2015; Palagina et al., 2017), a finding that is consistent among them is that component
421 cells by far outnumber pattern cells, with the former being ~25% of direction-tuned units and
422 the latter being about ~5% (with the rest being unclassified). With respect to the second
423 property, a well-known phenomenon likely affecting the strength of grating and plaid
424 responses is cross-orientation suppression (DeAngelis et al., 1992; Priebe and Ferster, 2006;
425 Li et al., 2006; Busse et al., 2009), which has been recently documented also in rodents (Self
426 et al., 2014; Alwis et al., 2016; Samonds et al., 2017). It consists in a reduction of the
427 response to the preferred oriented stimulus when this is presented together with other stimuli

428 with different orientations. This means that cross-orientation suppression could, in principle,
429 lead to diminished responses to plaids as compared to gratings. However, most studies
430 documenting this phenomenon mainly targeted V1, without distinguishing between pattern
431 and component cells. In addition, when focusing on studies of motion integration in rodents
432 (Juavinett and Callaway, 2015; Muir et al., 2015; Palagina et al., 2017), it was difficult to
433 draw any insight about the incidence of cross-orientation suppression in pattern and
434 component cells, because of methodological limitations (e.g., tuning curves normalization
435 and calcium imaging lacking spike-count-level information). This is why we turned to the
436 primate literature, finding hints of cross-orientation suppression being stronger in component
437 cells than in pattern cells (Smith et al., 2005; Rust et al., 2006).

438 Our hypothesis is that the combined effect of component cells being more numerous
439 than pattern cells, but also more sensitive to cross-orientation suppression, led the decoding
440 pool to become dominated by component cells in the case of training with gratings (G group)
441 and by pattern cells in the case of training with plaids (P group). In turn, this would
442 qualitatively explain the difference in terms of cross-priming found for the rats of the G and P
443 groups (Figure 2), as graphically illustrated in Figure 4A, B. Briefly, in the case of training
444 with gratings (Figure 4A, top), these stimuli would strongly activate both pattern (orange)
445 and component (green) cells (filled and unfilled neurons indicate, respectively, responsive
446 and unresponsive units). As such, the selection of the neuronal decoding pool by a
447 downstream decision neuron would not be biased towards either class of neurons (because of
448 no differences in their responsiveness). However, since the component cells substantially
449 outnumber the pattern cells, the decoding pool would contain more of the former (black-
450 boundary neurons) than of the latter (red-boundary neurons). This follows from the
451 assumption that the selection of the decoding pool is the result of a random sampling from the
452 subpopulation of all responsive units. This, in turn, is consistent with the idea that such
453 recruiting process is mediated by some form of plasticity similar to the reward-gated Hebbian
454 learning reviewed in (Roelfsema and Holtmaat, 2018). In the priming experiment, all the
455 neurons in the decoding pool would be active during presentation of the grating primes
456 (Figure 4A, middle), leading to the strong identity priming observed in Figure 2A (solid
457 curve). By contrast, most component cells in the pool would be strongly depressed by cross-
458 orientation suppression during presentation of the plaid primes (Figure 4A, bottom; empty
459 black-boundary neurons), and the few pattern cells in the pool (orange-filled, red-boundary
460 neurons), although active, would not be enough to affect the perception of the target stimulus.

461 Hence, the lack of cross-priming in the group of rats trained with gratings (Figure 2A, gray
462 curve).

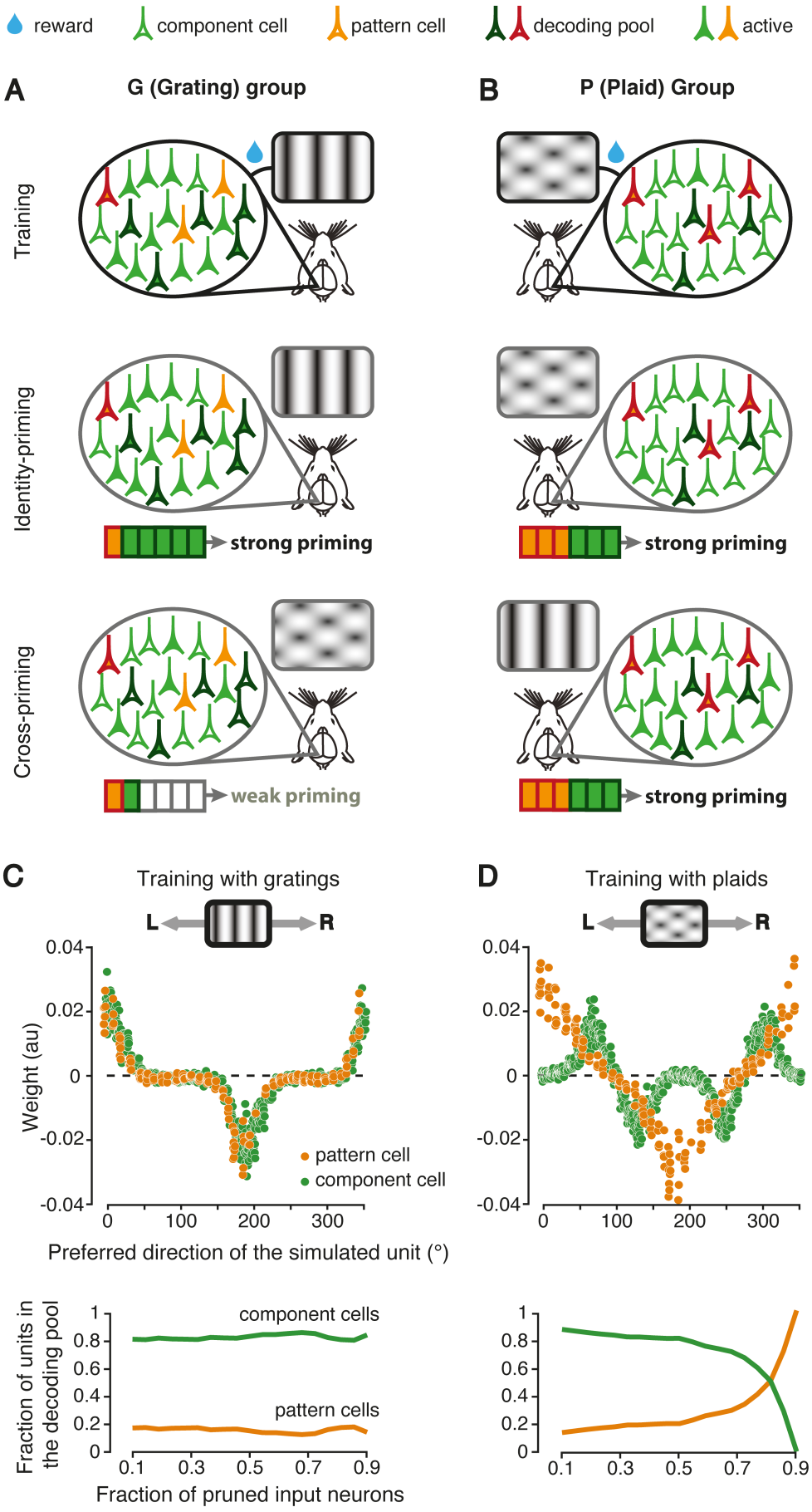

Figure 4. Simulating a scenario where training with either gratings or plaids leads to a decoding pool enriched of either component or pattern cells. (**A**) Cartoon illustrating how training with gratings would lead to the selection of a decoding pool enriched of component cells, under the assumption that: 1) component cells are more numerous than pattern cells; and 2) cross-orientation suppression is stronger for component than pattern cells. The sketched pyramidal neurons represent either component (green) or pattern (orange) cells. Filled and unfilled neurons indicate, respectively, responsive and unresponsive units. Black- and red-boundary neurons indicate the cells that the decision neuron learned to rely upon to discriminate the rightward- from the leftward-drifting gratings (i.e., the cells in the decoding pool). The grating stimuli activate equally strongly the component and pattern cells, but, being the former more numerous, the decoding pool is mainly composed of component cells (top). When tested with gratings, the cells in the decoding pool are strongly activated (middle), but, when they are tested with plaids, they are only weakly activated (bottom), because of cross-orientation suppression. (**B**) Cartoon illustrating how training with plaids would lead to the selection of a decoding pool enriched of pattern cells. Because of cross-orientation suppression, component cells are weakly activated by plaids, thus the decoding pool is enriched of pattern cells (top). As a result, the decoding pool is strongly activated when presented with both plaids (middle) or gratings (bottom). (**C**) Top: weights assigned to a mixed population of component (green) and pattern (orange) cells, as a function of their preferred direction, by a logistic classifier that was trained to discriminate a 0º- (rightward) from a 180º-drifting (leftward) grating. Bottom: The proportion of component (green) and pattern cells (orange), initially set to, respectively, 80% and 20% of the total, remained unchanged when weights with increasingly larger magnitude were progressively set to zero (i.e., pruned from the decoding pool). (**D**) Top: same as in C (top) but for a logistic classifier trained to discriminate a 0º- (rightward) from a 180º-drifting (leftward) plaid. Because of cross-orientation suppression, the classifier learned to assign weights with lower magnitude to the component cells. Bottom: as a result, when the input connections to the classifier were made increasingly sparser (by pruning weights with progressively larger magnitude), the proportion of pattern cells in the decoding pool (orange) reached and overtook the proportion of component cells (green).

In the case of training with plaids (Figure 4B, top), these stimuli would strongly activate the population of pattern cells (orange-filled neurons) but only weakly excite the component cells (green-filled neurons), because of cross-orientation suppression. This would lead to a strong bias towards the recruitment of pattern cells in the decoding pool (red-boundary neurons) by a downstream decision neuron. When tested with prime stimuli, such pattern-enriched pool would respond with a similar intensity to both kinds of primes (grating and plaids; Figure 4B, middle and bottom panels respectively), leading to similar priming curves in both identity- and cross-priming conditions, as shown in Figure 2B (solid vs. gray curve). This would account for the shared representation of global motion direction observed for rats trained with plaids.

To quantitatively test whether the mechanistic account hypothesized in the previous paragraphs could explain our findings, we built a computational model where a decision neuron had to select his afferent units from a mixed population of component and pattern cells, in order to discriminate the direction of either drifting gratings or plaids. The relative proportion of simulated component (80%) and pattern (20%) cells roughly matched that

found, on average, across rodent visual areas V1, LM and RL (Juavinett and Callaway, 2015; Muir et al., 2015; Palagina et al., 2017). Each unit was simulated as a Poisson spiking neuron, whose average firing rate as a function of direction was defined by a von Mises function (Kohn and Movshon, 2004; Matteucci et al., 2019) having a peak that was randomly sampled across the [0º 350º] direction axis (see Materials and methods for details).

In addition, to simulate cross-orientation suppression in component cells, their peak responses to plaids were set to half their peak responses to gratings. On the other hand, pattern cells were assumed to be unaffected by cross-orientation suppression. As for the simulation of Figure 3, the decision neuron consisted in a logistic classifier that was trained to discriminate between 0º- and 180º-drifting stimuli (i.e., leftward vs. rightward motion). This classifier simply performed a weighted sum over the inputs provided by all the simulated component and pattern cells, followed by the application of a sigmoidal nonlinearity. As a result of training, the weights became adjusted in such a way to maximize the classification accuracy (eventually attaining 100% in such a simple motion discrimination task).

When trained in the grating discrimination task (to simulate the training regime of the G group), the classifier learned to rely more heavily on those motion detectors (no matter whether component or pattern cells) whose preferred direction was close to that of the training stimuli. This is shown in Figure 4C (top), where the weights of the simulated units as a function of their preferred direction are reported. For both the component (green dots) and pattern (orange dots) cell populations, the most informative neurons were those with preferred direction close to 0º (rightward-drifting gratings) and 180º (leftward-drifting gratings), while the units tuned around the vertical drift direction (i.e., 90º and 270º) were assigned close-to-zero weights. Given these weight distributions, we simulated different degrees of sparsity constraints on the connectivity of the decision neuron. This was done by pruning input connections with progressively larger weight magnitude, thus gradually reducing the size of the decoding pool. However, given the closely matching weight magnitudes of the component and pattern cells, the level of pruning did not alter their relative proportion in the decoding pool – this proportion remained the same as in the original population (i.e., 80% vs. 20%; Figure 4C, bottom). This confirmed the intuition (see Figure 4A) that training with gratings, even in presence of asymmetric cross-orientation suppression (i.e., affecting component but not pattern cells), leads to a decoding pool that simply reflects the proportion of component and pattern cells of the overall cortical population and, as such, is component-enriched.

A very different scenario emerged when we simulated the training of the P group in the plaid discrimination task (see Figure 4D). The weight distribution learned by the classifier for the pattern cell population (top, orange dots) was the same as in the grating discrimination task. This is because our simulated pattern cells were by definition immune to cross-orientation suppression. On the other hand, the weight distribution for the component cell population (green dots) was very different from that obtained in the grating discrimination task. First, since these cells responded to the components of the plaids (i.e., their constituent gratings), the classifier learned to assign larger weights to those units with preferred direction at ±60º (i.e., half plaid cross-angle) with respect to the global directions of the leftward- and rightward-drifting plaids (same as for the simulations shown in Figure 3C). In addition, because the simulated components cells were affected by cross-orientation suppression, the classifier learned to rely less on component than on pattern cells, thus assigning lower weights to the former than to the latter (compare the absolute height of the peaks in the distributions of green and orange dots in Figure 4D, top). As a result, when the sparsity of the connections to the decision neuron was increased, by leaving in the decoding pool only inputs with progressively larger weight magnitude, the proportions of component and pattern cells in the pool followed opposite, mirror trends (Figure 4D, bottom). While the former decreased (green curve), the latter increased (orange curve), eventually leading to a reversal of the fraction of component and pattern cells in the decoding pool when the decision neuron was pruned of 90% of its potential inputs. This confirmed the intuition (see Figure 4B) that cross-orientation suppression can, at least in principle, strongly bias the recruitment of pattern cells in the decoding pool, under the constraint of sparse connectivity to the decision neurons, thus leading to a pattern-enriched representation despite the prevalence of component cells in the overall cortical population. As a control experiment, we repeated the whole simulation without any cross-orientation suppression. As expected, this yielded to a component-enriched representation for both the simulated G and P groups (data not shown).

Simulating a scenario where a decision neuron reading out a pattern representation fails to be activated by plaids, if originally trained to discriminate drifting gratings.

Despite the plausibility of the mechanism illustrated in the previous section, the key assumption of having weaker cross-orientation suppression on pattern cells than on component cells rests on hints from the primate literature only and has never been directly demonstrated in rodents. In addition, in our simulations, the decision neurons drew their

571 inputs from a mixed population of pattern and component cells. That is, we assumed the
572 decision neuron to pool from different stages of a putative motion processing hierarchy.
573 Considering primates, this assumption is clearly at odd with the higher functional and
574 anatomical rank of MT, with respect to V1, along the dorsal stream (Born and Bradley, 2005;
575 Orban, 2008). In the case of rodents, it is still unclear whether a similar hierarchy of dorsal
576 areas exists, but at least one study has reported extra-striate area RL to be richer of pattern
577 cells than V1 (Juavinett and Callaway, 2015). In addition, although an anatomical hierarchy
578 of motion processing stages as structured as the one found in primates may not exist in
579 rodents, pattern cells distributed over striate and extrastriate cortex could still sit above
580 component cells along the functional motion processing chain. In fact, pattern cells, given
581 their ability to encode motion direction in a shape-independent way, would behave as better
582 motion detectors than component cells in virtually any visually guided behavior. As such,
583 motion information could still be preferentially routed from visual cortical areas (e.g., V1,
584 RL, LM) to higher-order decision centers (i.e., frontal and parietal cortices) mainly via
585 pattern cells. This possibility is consistent with the well-established ability of distinct
586 subpopulations, within mouse V1, to selectively make (receive) target-specific projections
587 with (from) downstream (upstream) areas (Gao et al., 2010; Matsui and Ohki, 2013;
588 Glickfeld et al., 2013; Ji et al., 2015; D'Souza et al., 2019). In addition, it is consistent with a
589 very recent study showing that multiple visual areas (V1, LM and AL) are causally involved
590 in coding stimulus orientation and contrast (Jin and Glickfeld, 2020) – a demonstration that
591 the representation of key visual features is distributed among neuronal populations within
592 distinct visual areas.
593

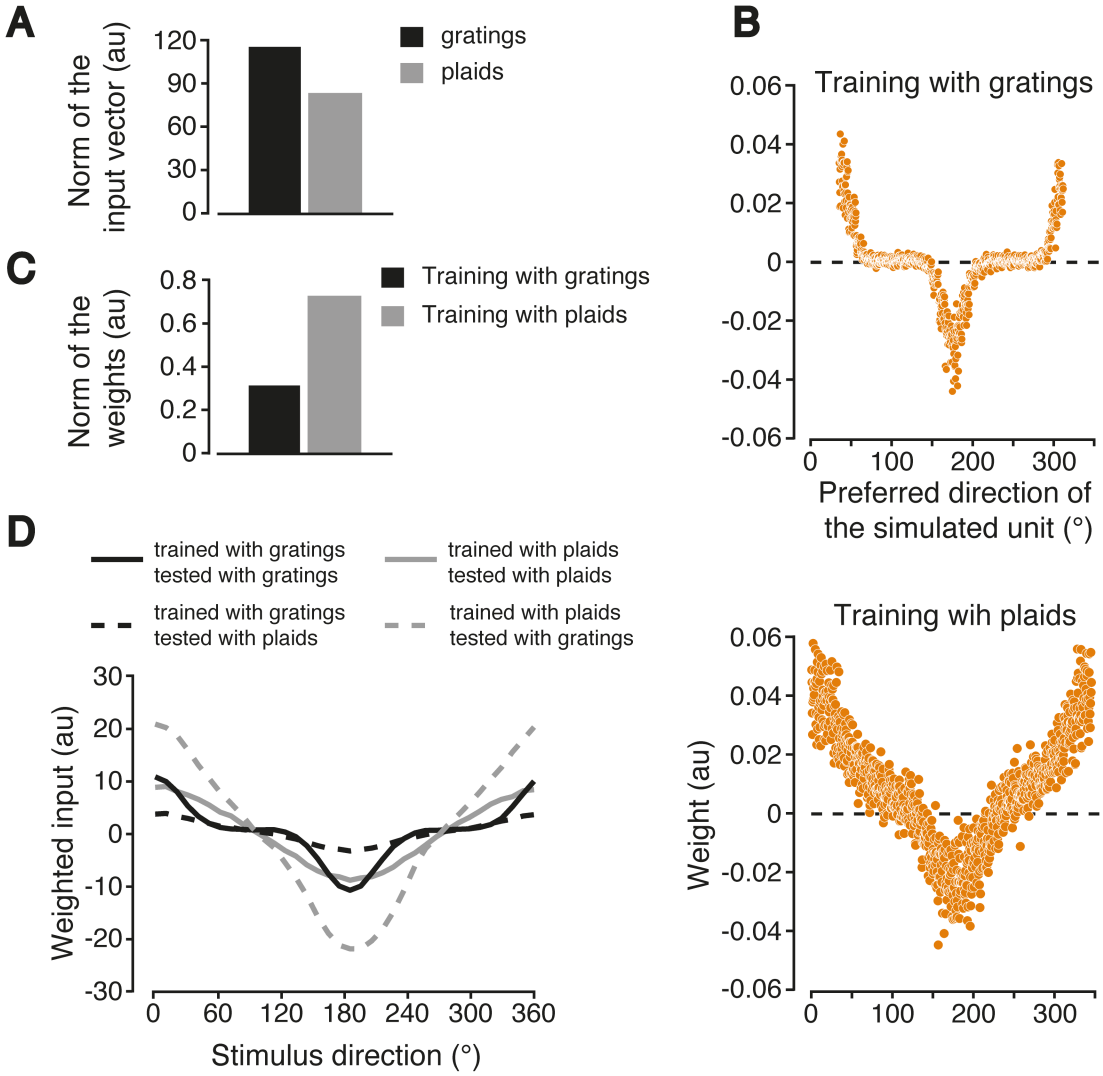

Figure 5. Simulating a scenario where a decision neuron reading out a population of pattern cells fails to be strongly activated by drifting plaids, when originally trained to discriminate drifting gratings. (**A**) L2 norms of the population vectors fed as inputs to a decision neuron (simulated as a logistic classifier with L2 regularization) that was trained to discriminate either a 0º- from 180º-drifting grating (black) or a 0º- from 180º-drifting plaid (gray). The classifier received inputs from a population of pattern cells. Each bar reports the mean of the norms of the input populations vectors produced by the 0º- and 180º-drifting stimuli. (**B**) Weights assigned by the logistic classifier to the population of pattern cells as a function of their preferred direction, in case of training with gratings (top) and plaids (bottom). (**C**) L2 norms of the weights shown in B. (**D**) Weighted inputs to the logistic classifier, originally trained to discriminate either gratings (black curves) or plaids (gray curves), when the population of simulated pattern cells was presented with drifting stimuli, homogeneously spanning the [0º 360º] range of directions. Such stimuli were either of the same kind (solid curves) or of a different kind (dashed curves) of those used during training. For instance, a classifier originally trained with plaids was tested with either plaids (gray, solid curve) or gratings (gray, dashed curve).

In light of these considerations, an alternative scenario to interpret our findings is one where: i) decision neurons receive inputs mainly from pattern cells, regardless of the motion

discrimination task to be performed (i.e., the decoding pool is, by "construction", pattern enriched); and ii) pattern cells are as sensitive to cross-orientation suppression as component cells are. The question is whether these assumptions are consistent with the difference in the magnitude of cross-priming produced by plaids on the rats of the G group (Figure 2A) and by gratings on the rats of the P group (Figure 2B). To account for this difference, we reasoned that pattern cells connected to a given decision neuron could fire less in response to plaids (because of cross-orientation suppression) than in response to gratings. This could lead the decision neuron to form stronger synaptic connections with its afferent pattern cells in the case of training with plaids than with gratings, under the assumption that some compensatory mechanisms actively keep the weighted input to the decision neuron around a target setpoint. Such compensatory process would be fully consistent with the well-known role played by homeostatic plasticity in cortex, where the overall synaptic strength scales as a function of the magnitude of the input, so as to maintain the average firing rate of cortical neurons within a given range (Turrigiano and Nelson, 2000; Turrigiano, 2008; Hengen et al., 2013).

To verify the plausibility of these intuitions, we simulated a downstream decision neuron reading out the representation conveyed by a population of pattern cells with strong cross-orientation suppression. As done in the previous section, we implemented the decision neuron as a logistic classifier with a regularization term on the L2 norm of its "synaptic" weights, so as to simulate the effect of homeostatic plasticity. The classifier was trained to discriminate either gratings or plaids drifting in opposite directions (i.e., 0º vs. 180º motion direction). As a result of the cross-orientation suppression, the L2 norm of the population vectors fed as inputs to the classifier was larger for the gratings than for the plaids (Figure 5A). This led the magnitude of the weights to become larger in the case of training with the plaids than with the gratings (Figure 5B), with the L2 norm of the weights' vector being more than twice as large in the former case (Figure 5C).

This had the "homeostatic" effect of nearly equalizing the magnitude of the weighted inputs to the classifier, when this was fed with the same kind of stimuli that were used for training. As shown in Figure 5D, the weighted inputs resulting from presenting drifting gratings to the classifier that was trained to discriminate grating motion direction (solid black curve) were very close to the weighted inputs resulting from presenting drifting plaids to the classifier that was trained to discriminate plaid motion direction (solid gray curve). This would explain the strong identity priming observed for the rats of both the G and P groups in our experiment (Figure 2, black curves). At the same time, the large weights' magnitude

resulting from the training with the plaids also guaranteed a very strong weighted input in the case of presentation of the grating stimuli (dashed gray curve in Figure 5D). This would explain the strong cross-priming observed for the rats of the P group (Figure 2B, gray curve). By contrast, the much smaller weights resulting from training with the gratings yielded a near-zero weighted input in the case of presentation of the plaid stimuli (dashed black curve in Figure 5D). This would explain the very small cross-priming observed for the rats of the G group (Figure 2A, gray curve). A plaid prime stimulus would simply be too weak (because of cross-orientation suppression) to activate the decision neuron through the weak, grating-adapted synaptic weights.

Conclusions and implications

Although speculative in nature, the two explanations detailed in the previous paragraphs and backed up by our simulations propose an account for the behavioral data reported in our study. Importantly, they both rest on well-defined physiological assumptions. As such, they give rise to alternative hypotheses about the neural mechanisms underlying the processing of motion information that could be tested experimentally. For instance, the first explanation (Figure 4) would be supported by observing cross-orientation suppression acting way more strongly on component than on pattern cells in rodent visual cortex. On the other hand, the second explanation (Figure 5) would be corroborated by observing that cross-orientation suppression affects equally strongly pattern and component cells, and by finding a projection-specific enrichment in the proportion of pattern cells relaying visual information to decision making centers, such as posterior parietal cortex (PPC) (Raposo et al., 2014; Licata et al., 2017; Nikbakht et al., 2018; Odoemene et al., 2018).

In conclusion, our study not only yields behavioral evidence of motion integration in rodents, but also provides solid grounding for future investigations aimed at dissecting the neuronal circuits underlying integration of local motion cues into global motion percepts. In fact, as highlighted in a recent perspective (Rasmussen and Yonehara, 2017), a behavioral task involving direction discrimination of gratings and plaids is a necessary ingredient of future experiments aimed at establishing a correlational and/or causal link between pattern-like responses observed in rodent visual cortex and integrated motion perception.

675 ## Materials and methods

676 **Animal procedures**

677 We trained 21 male Long Evans rats (Charles River Laboratory) in a motion direction
678 discrimination task. Upon arrival in the lab, rats weighed ~250 g, and they grew up to ~500 g.
679 Animals started training during ~ 7th postnatal week. During the experimental period, they
680 had free access to food, while their access to water was restricted. Their daily liquid intake
681 included 5 – 15 ml of a 1:4 juice-water solution, plus an ad libitum water access for one hour
682 after training. Training sessions lasted 50 – 70 minutes and took place 5 days per week. All
683 animal procedures were conducted in accordance with the international and institutional
684 standards for the care and use of animals in research and were approved by the Italian
685 Ministry of Health and after consulting with a veterinarian (Project DGSAF 25271, submitted
686 on December 1, 2014 and approved on September 4, 2015, approval 940/2015-PR).

687 **Behavioral apparatus and visual stimuli**

688 The behavioral rig consisted of two racks, each equipped with three operant boxes to allow
689 training a batch of six rats simultaneously (Zoccolan, 2015; Zoccolan and Di Filippo, 2018).
690 In each box, one of the walls bore a 3 cm-diameter hole, so that a rat could extend its head
691 outside the box and face the stimulus display (a LCD monitor ASUS® Ve228 located at 30
692 cm from the viewing hole). The box was equipped with three stainless-steel feeding needles
693 (Cadence Science®), located right outside the viewing hole, and serving as response ports
694 and for reward delivery. To this end, each needle was connected to a led-photodiode pair to
695 detect when the nose of the animal approached and touched it. The two ports positioned to
696 the right and to the left of the hole were connected to two computer-controlled syringe pumps
697 (New Era Pump Systems NE-500®) for delivery of liquid reward, while the central port
698 served exclusively to trigger the onset of each behavioral trial. Each rat learnt to extend its
699 head through the viewing hole, lick the central needle to trigger stimulus presentation and
700 then lick either the left or right port to report the identity of the visual stimulus presented in
701 the current trial. In case of correct response, the reward was delivered through the feeding
702 needle. In case of an incorrect choice, a 1-3 s timeout period started, with the stimulus display
703 flickering from black to middle gray at a rate of 15 Hz (during this period, a "failure" sound
704 was also played). Stimulus presentation, response collection and reward delivery were
705 controlled via workstations running open source MWorks software
706 (https://mworks.github.io/).

As explained in the Results, the rats were divided in two groups. The animals in the G group were trained to discriminate gratings drifting horizontally in opposite directions, i.e., 180° (leftward) vs. 0° (rightward). The rats of the P group were trained to discriminate two drifting plaids, whose global motion direction was, again, either 180° or 0º. The grating stimuli consisted in full-field, full-contrast, sine wave drifting gratings with a temporal frequency of 2 Hz and a spatial frequency of 0.04 cycles/°. The plaid stimuli were constructed by superimposition of two half-contrast gratings (again 0.04 cycles/° and 2 Hz) with a motion direction difference of 120° (i.e., 120° plaid cross-angle). In the experiments with the priming paradigm (see below), the drift direction of the prime stimuli (either gratings or plaids) was randomly sampled in each trial from 19 possible directions (i.e., from 0° to 180° in steps of 10; see Figure 1).

Experimental design - Training phase

As soon as a rat licked the central response port, the target stimulus appeared (either a grating or a plaid depending on the animal's experimental group) and remained on screen for 2 s. To prevent rats from making very quick, impulsive responses, a trial was aborted if the animal's reaction time was lower than 300 ms. In such a case, the animal's response was not evaluated (neither reward or time-out was administered), the stimulus was immediately turned off, and a brief tone was played. Such "too fast" trials were also excluded from the analysis. Similarly, trials in which the rat responded more than 2 s after the offset of the stimulus were considered "ignored" and excluded from the analysis. No reward was delivered in these invalid trials. In order to accomplish the task and receive the reward, the rat had to reach and lick the response port matching the global motion direction of the target stimulus. Correct execution of such task was rewarded equally for both directions during each experimental session. In correct trials, the target stimulus remained on the screen for the whole reward delivery period, so as to strengthen the operant association between stimulus response and reward. On the other hand, when the animal provided an incorrect response, reward was not delivered, the stimulus was immediately turned off and the timeout period started (see previous section).

Experimental design - Priming paradigm

In the priming paradigm, a prime stimulus was shown to the animal before the target stimulus. The prime duration was 75 ms, the inter-stimulus interval (ISI, i.e., the interval separating the offset of the prime from the onset of the target) was also 75 ms and the target

duration was 750 ms. As in the training phase, “too fast” or “ignored” trials were excluded from the analysis. Only, a trial was defined as “ignored” if the rat responded more than 1 s after the onset of the target stimulus. As a result, the allowed response window extended from 300 to 1000 ms from target onset. As in the training phase, an animal, in order to obtain the reward, had to reach and lick the response port (right or left) corresponding to the global motion direction of the target. Accordingly, no feedback was ever provided to the rat regarding the motion direction of prime stimuli. In this paradigm, the target was not kept on screen during the reward, because there was no longer any need to favor the association between response, stimulus, and reward. Only animals maintaining a performance in the training task greater that 75% for 4 consecutive days were tested with this priming paradigm.

The rationale of this design rests on well-established findings in the human psychophysics literature (Bar and Biederman, 1998; Leopold et al., 2001; Kanai and Verstraten, 2005; Kravitz et al., 2010), where presenting an “adapter” before a “test” stimulus has been shown to bias the perception of the test, depending on two key factors: the duration of the adapter and the inter stimulus interval (ISI) between adapter and target presentation. When the bias induced by the adapter attracts the perceptual choices towards the identity of the adapter itself, this effect is called “priming”. Vice versa, when it repels the perceptual choices away from the identity of the adapter, it is named “adaptation after-effect”. Our group previously shown that brief presentation of a static shape (~50 ms), followed by a short ISI (66 ms), is able to induce a strong and robust priming effect on rat response to a target shape (Tafazoli et al., 2012). Here, we adapted this paradigm to moving stimuli, and we relied on previous motion priming studies in humans (Kanai and Verstraten, 2005) to select the timing parameters of the task, in the attempt of inducing a strong priming effect.

Analysis of behavioral data

Only rats displaying a strong identity-priming effect where included in the analysis described in the main text. Quantitatively, this corresponded to setting a threshold on the absolute priming magnitude in the identity priming condition amounting to 5%. Priming magnitude was computed averaging together the mean values of the absolute difference between the left and right extremes (4 points per side) of each priming curve with respect to the neutral prime condition (insets in Figure 2). The enforcement of such criterion led to the rejection of one rat per group, bringing the number of rats included in the analysis to 10 animals for the G group

770 and to 9 animals for the P group out of the original 11 animals trained in grating direction
771 discrimination and 10 trained in plaid direction discrimination.

772 To statistically compare the identity- and cross-priming curves obtained for each
773 group of rats (solid and dashed curves in Figure 2) we performed a bootstrap analysis, in
774 which the recorded behavioral sessions were resampled 50 times with replacement for each
775 animal independently. This gave us the possibility to estimate a bootstrap standard deviation
776 for both the average identity- and cross-priming curves of Figure 2, as well as for the average
777 priming magnitudes computed as described above (insets in Figure 2). Bootstrap standard
778 deviations were then used to compute normal 95% confidence intervals for the
779 aforementioned quantities (displayed in Figure 2 as shaded regions around the priming curves
780 and as error bars in the bar plot shown in the insets) (Efron and Tibshirani, 1986). In
781 computing confidence intervals for the 19 points of a priming curve, the critical value
782 corresponding to the chosen confidence level was adjusted for multiple comparisons using
783 Bonferroni correction.

784 **Computational modeling**

785 To interpret the results of our psychophysical tests, we simulated a decision neuron reading
786 out the activity of a simulated population of either component or pattern cells fed with either
787 grating or plaid stimuli. Three different simulations were performed to test the consistency of
788 our findings with three possible scenarios concerning the tuning of rat visual neurons for
789 motion direction and the choice of the decoding pool by the decision neuron. These
790 simulations have been already described in the Results and in the legends of Figures 3, 4 and
791 5. Below, we explain some additional technical details about how we modeled the
792 populations of simulated component and pattern cells and how we implemented the logistic
793 classifier used to simulate the decision neuron.

794 *Simulations to check the consistency of the priming curves observed for the P group with a*
795 *pattern-based representation of global motion direction*

796 To check whether the shape of the priming curves observed for the rats of the P group (Figure
797 2B) was more consistent with a component-like or a pattern-like representation, we trained a
798 logistic classifier to solve the same motion discrimination task that was administered to the
799 rats (i.e., 0º- vs. 180º-drifting plaids), based on the responses of a simulated population of
800 either component of pattern cells (Figure 3). We then tested how the trained classifier would
801 decode the full range of drifting plaids and gratings used to obtain, respectively, the identity-

802 and cross-priming curves in Figure 2B. To simulate the tuning for local and global motion
803 direction of the populations of component and pattern cells, we used 24 Von Mises functions
804 (Kohn and Movshon, 2004; Matteucci et al., 2019) centered at equispaced angles along the
805 circle (spaced by 15°). The von Mises functions, which are the circular analogs of Gaussian
806 functions, have a width that is controlled by the parameter *k*, which, in turn, is equivalent to
807 the inverse of the variance of a Gaussian distribution (Berens, 2009). The peak value of the
808 functions (and thus of the tuning curves) was set to 1 for all the simulated units.

809 For a pattern cell, the simulated tuning curve was the same regardless of whether the
810 input stimulus was a plaid or a grating stimulus (compare matching rows in the top and
811 bottom panels of Figure 3B). That is, by construction, each simulated pattern cell responded
812 to the global direction of the plaid stimuli. Conversely, for a component cell, the simulated
813 tuning curve was defined by a single Von Mises function in case of presentation of the
814 grating stimuli (Figure 3A, top), but was defined by the superimposition of two von Mises
815 functions (with the peaks being 120º apart) in case of presentation of the plaid stimuli (Figure
816 3A, bottom). That is, by construction, each simulated component cell responded to the local
817 directions of the constituent gratings of the plaid stimuli, rather than to the global direction of
818 the plaid. For both the simulated pattern and component cells, the Von Mises functions were
819 summed to a constant background activity. In addition, to emulate the variability of neuronal
820 firing in response to identical stimuli, in each simulated trial, the actual response to a given
821 stimulus was affected by Gaussian noise with zero mean and $\sigma = 0.25$. The *k* parameter of the
822 Von Mises functions of the simulated pattern and component cells was set to 7 in the mean
823 simulation shown in Figure 3, while it was allowed to range between 0.5 and 11 in the more
824 extended simulations of Figure 3–figure supplement 1. The ratio between the peak of the
825 tuning curves and the background rate was set to 10.

826 To model the training received by the rats in our experiment, we sampled for 500
827 times the responses of the whole population of either pattern or component cells to each of
828 the 0º- and 180º-drifting stimuli (either grating or plaids) used during the training phase. We
829 then trained a logistic regression classifier to discriminate the two sets of 0º and 180º
830 responses using gradient descent (implemented by the Matlab function "fminunc") and
831 including and L2 regularization term in the cost function (whose parameter lambda was set to
832 1). The weights resulting from such training are those shown in Figure 3C and E. Finally, we
833 fed to the classifier grating and plaid stimuli spanning the full range of possible global motion

834 directions (from 0º to 345º in steps of 15º) and we plotted the probability for each class of
835 stimuli to be classified as moving rightward as a function of its direction (Figure 3D and F).

836 *Simulations to explore the mechanisms that could lead to a strong cross-priming only in case*
837 *of training with plaid stimuli – scenario #1*

838 To obtain a proof of principle that the mechanisms illustrated in Figure 4A, B could lead to a
839 decoding pool enriched of pattern cells in case of training with plaids, we carried out a
840 second simulation. As before, we trained a logistic regression classifier in the same motion
841 direction discrimination task that was administered to our animals. This time, however, the
842 response properties of the simulated component and pattern cells, as well as their relative
843 proportion, better matched either the known properties derived from the rodent literature
844 (Juavinett and Callaway, 2015; Muir et al., 2015; Palagina et al., 2017) or those inferred
845 based on the monkey literature (Smith et al., 2005; Rust et al., 2006). First, the simulated
846 population of pattern and component cells was much larger (i.e., 1000 units). It was
847 composed of Poisson firing neurons with either "component" or "pattern" tuning curves, built
848 in the same way as described in the previous section. Second, their proportion was 80% and
849 20% respectively, so as to match the highest ratio of pattern to component cells observed in
850 rodent visual cortex (Juavinett and Callaway, 2015). As in the previous simulation, we used
851 Von Mises functions to define the tuning curves of component and pattern cells (see
852 description in the previous section). In this case however, the preferred directions of the
853 simulated neurons were not equispaced but drawn randomly from a uniform distribution over
854 the circle. Baseline value of tuning curves was set to 2 spikes/second. Von Mises function of
855 random amplitude (normally distributed around 8 spikes/s with standard deviation of 1 spike
856 per second) were added to this baseline. The firing rate of the units in each trial was drawn
857 from a Gaussian distribution with mean equal to the value set by the tuning curves and
858 standard deviation of 2 spikes/s. The width (i.e., the parameter k; see previous paragraph) of
859 the Von Mises functions was adjusted in such a way that the Orientation Selectivity Index
860 (OSI) of the resulting population of component cells was distributed according to a Gaussian
861 with a mean of 0.7 and a standard deviation of 0.1, while the Direction Selectivity Index
862 (DSI) was distributed according to a Gaussian with a mean of 0.6 and a standard deviation of
863 0.2. OSI and DSI are standard measures of orientation and direction tuning, whose definition
864 can be found, for instance, in (Niell and Stryker, 2008; Vermaercke et al., 2014; Matteucci et
865 al., 2019; Matteucci and Zoccolan, 2020).

To account for the imperfect cross-angle invariance documented by (Palagina et al., 2017) we enlarged the width of Von Mises functions used to simulate the tuning of pattern cells to plaids by dividing the *k* parameter previously used to define their tuning to gratings (see previous paragraph) by a factor 4. This made the responses of our simulated pattern cells better matched to the known properties of mouse pattern cells, reproducing their tendency to have broader tuning curves when tested with plaids than with gratings, especially when the plaids have a large cross-angle (such as the one used in our study, i.e. 120°).

Finally, we simulated cross-orientation suppression in component cells – that is, we imposed that the peak responses of component cells to the plaids were half of their peak responses to the gratings, while pattern cells were implemented as being fully unaffected by cross-orientation suppression (i.e., same peak responses to plaids and gratings). This scenario was simulated because our goal was to test the hypothesis that, if cross-orientation suppression affected strongly component cells but not pattern cells, then the decision neuron would learn to preferentially connect with the latter, in the case of training with the plaid stimuli.

To model the training received by the rats in our experiment, we sampled for 200 times the responses of the mixed population of pattern or component cells to each of the 0º- and 180º-drifting stimuli (either grating or plaids) used during the training phase. We then trained a logistic regression classifier to discriminate the two sets of 0º and 180º responses using gradient descent (implemented by the Matlab function "fminunc") and including and L2 regularization term in the cost function (whose parameter lambda was set to 1). The weights resulting from such training are those shown in Figure 4C and D (top). Finally, we simulated a scenario where, as a result of this training, the decision neuron would maintain only the strongest of its synaptic connections with sensory neurons encoding the drifting stimuli. To incorporate this sparseness constraint on the connectivity of the decision neuron, we progressively pruned the weakest synaptic weights by applying a quantile-based thresholding to their magnitude after training (i.e., by setting to zero any weight below the chosen quantile of the original weight magnitude distribution). We then quantified the proportion of pattern and component cells that survived the pruning and remained in the decoding pool of the decision neuron as a function of the quantile used as a threshold (Figure 4C and D, bottom). As a control, the whole simulation was also run without incorporating cross-orientation suppression in the responses of component cells.

Simulations to explore the mechanisms that could lead to a strong cross-priming only in case of training with plaid stimuli – scenario #2

Here, we simulated an alternative scenario where a decision neuron (modeled, again, as a logistic classifier) is connected to a pool of sensory neurons made exclusively of pattern cells that are strongly affected by cross-orientation suppression. As such, the parameters of the simulations were the same as those described in the previous section, with only two notable differences: 1) no component cells were included in the decoding pool, but only pattern cells; 2) cross-orientation suppression affected pattern cells instead of components cells, and its impact was twice as strong as that of the previous stimulation (i.e., peak responses to plaids were 25% of peak responses to gratings). The training of the classifier was the same as described in the previous section. Note that the L2 regularization term in the cost function played the role of a homeostatic constraint on the overall weights' magnitude. Again, we compared the weights' distributions resulting from training with plaids and gratings (Figure 5B) and we also quantified the magnitude of weighted input (i.e., sensory "evidence") to the decision neuron, depending on the training and prime stimuli (Figure 5D).

Acknowledgments. This work was supported by a European Research Council Consolidator Grant (DZ, project n. 616803-LEARN2SEE). We thank Daniele Bertolini for his help in developing and building the rigs for the behavioral experiments, and we thank Sofia Erica Rossi and Marco Salluzzo for their help in training rats in the motion discrimination task.

Competing interests. None of the authors has financial and non-financial competing interests of any nature.

References

Adelson EH, Movshon JA (1982) Phenomenal coherence of moving visual patterns. Nature 300:523–525.

Alemi-Neissi A, Rosselli FB, Zoccolan D (2013) Multifeatural Shape Processing in Rats Engaged in Invariant Visual Object Recognition. J Neurosci 33:5939–5956.

Alwis DS, Richards KL, Price NSC (2016) Masking reduces orientation selectivity in rat visual cortex. J Neurophysiol 116:2331–2341.

Bar M, Biederman I (1998) Subliminal Visual Priming. Psychol Sci 9:464–468.

Berens P (2009) CircStat: A MATLAB Toolbox for Circular Statistics. J Stat Softw 31.

Born RT, Bradley DC (2005) Structure and function of visual area MT. Annu Rev Neurosci 28:157–189.

Busse L, Wade AR, Carandini M (2009) Representation of Concurrent Stimuli by Population Activity in Visual Cortex. Neuron 64:931–942.

Carandini M, Churchland AK (2013) Probing perceptual decisions in rodents. Nat Neurosci 16:824–831.

Chen T-W, Wardill TJ, Sun Y, Pulver SR, Renninger SL, Baohan A, Schreiter ER, Kerr RA, Orger MB, Jayaraman V (2013) Ultrasensitive fluorescent proteins for imaging neuronal activity. Nature 499:295.

DeAngelis GC, Robson JG, Ohzawa I, Freeman RD (1992) Organization of suppression in receptive fields of neurons in cat visual cortex. J Neurophysiol 68:144–163.

Dell KL, Arabzadeh E, Price NSC (2018) Human-like perceptual masking is difficult to observe in rats performing an orientation discrimination task. PLOS ONE 13:e0207179.

Dell KL, Arabzadeh E, Price NSC (2019) Differences in perceptual masking between humans and rats. Brain Behav 9:e01368.

Djurdjevic V, Ansuini A, Bertolini D, Macke JH, Zoccolan D (2018) Accuracy of Rats in Discriminating Visual Objects Is Explained by the Complexity of Their Perceptual Strategy. Curr Biol 28:1005-1015.e5.

Douglas RM, Neve A, Quittenbaum JP, Alam NM, Prusky GT (2006) Perception of visual motion coherence by rats and mice. Vision Res 46:2842–2847.

D'Souza RD, Bista P, Meier AM, Ji W, Burkhalter A (2019) Spatial Clustering of Inhibition in Mouse Primary Visual Cortex. Neuron 104:588-600.e5.

Efron B, Tibshirani R (1986) Bootstrap Methods for Standard Errors, Confidence Intervals, and Other Measures of Statistical Accuracy. Stat Sci 1:54–75.

Fennema CL, Thompson WB (1979) Velocity determination in scenes containing several moving objects. Comput Graph Image Process 9:301–315.

Fenno L, Yizhar O, Deisseroth K (2011) The Development and Application of Optogenetics. Annu Rev Neurosci 34:389–412.

Gao E, DeAngelis GC, Burkhalter A (2010) Parallel Input Channels to Mouse Primary Visual Cortex. J Neurosci 30:5912–5926.

Ghodrati M, Alwis DS, Price NSC (2016) Orientation selectivity in rat primary visual cortex emerges earlier with low-contrast and high-luminance stimuli. Eur J Neurosci 44:2759–2773.

Girman SV, Sauvé Y, Lund RD (1999) Receptive Field Properties of Single Neurons in Rat Primary Visual Cortex. J Neurophysiol 82:301–311.

Glickfeld LL, Andermann ML, Bonin V, Reid RC (2013) Cortico-cortical projections in mouse visual cortex are functionally target specific. Nat Neurosci 16:219–226.

Harvey RJ, De'sperati C, Strata P (1997) The Early Phase of Horizontal Optokinetic Responses in the Pigmented Rat and the Effects of Lesions of the Visual Cortex. Vision Res 37:1615–1625.

Hengen KB, Lambo ME, Van Hooser SD, Katz DB, Turrigiano GG (2013) Firing Rate Homeostasis in Visual Cortex of Freely Behaving Rodents. Neuron 80:335–342.

Ji W, Gămănuţ R, Bista P, D'Souza RD, Wang Q, Burkhalter A (2015) Modularity in the Organization of Mouse Primary Visual Cortex. Neuron 87:632–643.

Jin M, Glickfeld LL (2020) Mouse Higher Visual Areas Provide Both Distributed and Specialized Contributions to Visually Guided Behaviors. Curr Biol 30:4682-4692.e7.

Juavinett AL, Callaway EM (2015) Pattern and Component Motion Responses in Mouse Visual Cortical Areas. Curr Biol 25:1759–1764.

Kanai R, Verstraten FAJ (2005) Perceptual manifestations of fast neural plasticity: Motion priming, rapid motion aftereffect and perceptual sensitization. Vision Res 45:3109–3116.

Kohn A, Movshon JA (2004) Adaptation changes the direction tuning of macaque MT neurons. Nat Neurosci 7:764–772.

Kravitz DJ, Kriegeskorte N, Baker CI (2010) High-Level Visual Object Representations Are Constrained by Position. Cereb Cortex 20:2916–2925.

Leopold DA, O'Toole AJ, Vetter T, Blanz V (2001) Prototype-referenced shape encoding revealed by high-level aftereffects. Nat Neurosci 4:89–94.

Li B, Thompson JK, Duong T, Peterson MR, Freeman RD (2006) Origins of Cross-Orientation Suppression in the Visual Cortex. J Neurophysiol 96:1755–1764.

Licata AM, Kaufman MT, Raposo D, Ryan MB, Sheppard JP, Churchland AK (2017) Posterior Parietal Cortex Guides Visual Decisions in Rats. J Neurosci 37:4954–4966.

Lisberger SG (2015) Visual Guidance of Smooth Pursuit Eye Movements. Annu Rev Vis Sci 1:447–468.

Luo L, Callaway EM, Svoboda K (2008) Genetic Dissection of Neural Circuits. Neuron 57:634–660.

Luo L, Callaway EM, Svoboda K (2018) Genetic Dissection of Neural Circuits: A Decade of Progress. Neuron 98:256–281.

Madisen L, Garner AR, Shimaoka D, Chuong AS, Klapoetke NC, Li L, Van Der Bourg A, Niino Y, Egolf L, Monetti C (2015) Transgenic mice for intersectional targeting of neural sensors and effectors with high specificity and performance. Neuron 85:942–958.

Marques T, Summers MT, Fioreze G, Fridman M, Dias RF, Feller MB, Petreanu L (2018) A Role for Mouse Primary Visual Cortex in Motion Perception. Curr Biol CB 28:1703-1713.e6.

Marr D (2010) Vision: a computational investigation into the human representation and processing of visual information. Cambridge, Mass: MIT Press.

1007 Marshel JH, Garrett ME, Nauhaus I, Callaway EM (2011) Functional Specialization of Seven
1008 Mouse Visual Cortical Areas. Neuron 72:1040–1054.

1009 Matsui T, Ohki K (2013) Target dependence of orientation and direction selectivity of
1010 corticocortical projection neurons in the mouse V1. Front Neural Circuits 7 Available
1011 at: https://www.frontiersin.org/articles/10.3389/fncir.2013.00143/full [Accessed
1012 January 26, 2018].

1013 Matteucci G, Marotti RB, Riggi M, Rosselli FB, Zoccolan D (2019) Nonlinear Processing of
1014 Shape Information in Rat Lateral Extrastriate Cortex. J Neurosci 39:1649–1670.

1015 Matteucci G, Zoccolan D (2020) Unsupervised experience with temporal continuity of the
1016 visual environment is causally involved in the development of V1 complex cells. Sci
1017 Adv 6:eaba3742.

1018 Muir DR, Roth MM, Helmchen F, Kampa BM (2015) Model-based analysis of pattern motion
1019 processing in mouse primary visual cortex. Front Neural Circuits 9 Available at:
1020 http://www.ncbi.nlm.nih.gov/pmc/articles/PMC4525018/ [Accessed April 24, 2017].

1021 Newsome W, Pare E (1988) A selective impairment of motion perception following lesions of
1022 the middle temporal visual area (MT). J Neurosci 8:2201–2211.

1023 Niell CM, Stryker MP (2008) Highly selective receptive fields in mouse visual cortex. J
1024 Neurosci 28:7520–36.

1025 Nikbakht N, Tafreshiha A, Zoccolan D, Diamond ME (2018) Supralinear and Supramodal
1026 Integration of Visual and Tactile Signals in Rats: Psychophysics and Neuronal
1027 Mechanisms. Neuron 97:626-639.e8.

1028 Nishida S, Kawabe T, Sawayama M, Fukiage T (2018) Motion Perception: From Detection to
1029 Interpretation. Annu Rev Vis Sci 4:501–523.

1030 Odoemene O, Pisupati S, Nguyen H, Churchland AK (2018) Visual Evidence Accumulation
1031 Guides Decision-Making in Unrestrained Mice. J Neurosci 38:10143–10155.

1032 Orban GA (2008) Higher Order Visual Processing in Macaque Extrastriate Cortex. Physiol
1033 Rev 88:59.

1034 Palagina G, Meyer JF, Smirnakis SM (2017) Complex Visual Motion Representation in
1035 Mouse Area V1. J Neurosci 37:164–183.

1036 Priebe NJ, Ferster D (2006) Mechanisms underlying cross-orientation suppression in cat
1037 visual cortex. Nat Neurosci 9:552–561.

1038 Raposo D, Kaufman MT, Churchland AK (2014) A category-free neural population supports
1039 evolving demands during decision-making. Nat Neurosci 17:1784–1792.

1040 Rasmussen R, Yonehara K (2017) Circuit Mechanisms Governing Local vs. Global Motion
1041 Processing in Mouse Visual Cortex. Front Neural Circuits 11:109.

1042 Roelfsema PR, Holtmaat A (2018) Control of synaptic plasticity in deep cortical networks.
1043 Nat Rev Neurosci 19:166–180.

1044 Rosselli FB, Alemi A, Ansuini A, Zoccolan D (2015) Object similarity affects the perceptual
1045 strategy underlying invariant visual object recognition in rats. Front Neural Circuits
1046 9:10.

1047 Rust NC, Mante V, Simoncelli EP, Movshon JA (2006) How MT cells analyze the motion of
1048 visual patterns. Nat Neurosci 9:1421–31.

1049 Salzman CD, Britten KH, Newsome WT (1990) Cortical microstimulation influences
1050 perceptual judgements of motion direction. Nature 346:174–177.

1051 Samonds JM, Feese BD, Lee TS, Kuhlman SJ (2017) Nonuniform surround suppression of
1052 visual responses in mouse V1. J Neurophysiol 118:3282–3292.

1053 Samonds JM, Lieberman S, Priebe NJ (2018) Motion Discrimination and the Motion
1054 Aftereffect in Mouse Vision. eNeuro 5.

1055 Self MW, Lorteije JAM, Vangeneugden J, Beest EH van, Grigore ME, Levelt CN, Heimel JA,
1056 Roelfsema PR (2014) Orientation-Tuned Surround Suppression in Mouse Visual
1057 Cortex. J Neurosci 34:9290–9304.

1058 Simoncelli EP, Heeger DJ (1998) A model of neuronal responses in visual area MT. Vision
1059 Res 38:743–761.

1060 Smith AT, Harris LR (1991) Use of plaid patterns to distinguish the corticofugal and direct
1061 retinal inputs to the brainstem optokinetic nystagmus generator. Exp Brain Res 86
1062 Available at: http://link.springer.com/10.1007/BF00228955 [Accessed November 23,
1063 2019].

1064 Smith MA, Majaj NJ, Movshon JA (2005) Dynamics of motion signaling by neurons in
1065 macaque area MT. Nat Neurosci 8:220–228.

1066 Solomon SS, Tailby C, Gharaei S, Camp AJ, Bourne JA, Solomon SG (2011) Visual motion
1067 integration by neurons in the middle temporal area of a New World monkey, the
1068 marmoset: Pattern motion sensitivity in middle temporal area of marmosets. J Physiol
1069 589:5741–5758.

1070 Stahl JS (2004) Using eye movements to assess brain function in mice. Vision Res
1071 44:3401–3410.

1072 Stirman JN, Townsend LB, Smith SL (2016) A touchscreen based global motion perception
1073 task for mice. Vision Res 127:74–83.

1074 Tafazoli S, Di Filippo A, Zoccolan D (2012) Transformation-Tolerant Object Recognition in
1075 Rats Revealed by Visual Priming. J Neurosci 32:21–34.

1076 Turrigiano GG (2008) The Self-Tuning Neuron: Synaptic Scaling of Excitatory Synapses.
1077 Cell 135:422–435.

1078 Turrigiano GG, Nelson SB (2000) Hebb and homeostasis in neuronal plasticity. Curr Opin
1079 Neurobiol 10:358–364.

1080 Vermaercke B, Gerich FJ, Ytebrouck E, Arckens L, Op de Beeck HP, Van den Bergh G
1081 (2014) Functional specialization in rat occipital and temporal visual cortex. J
1082 Neurophysiol 112:1963–1983.

Wuerger S, Shapley R, Rubin N (1996) “On the Visually Perceived Direction of Motion” by Hans Wallach: 60 Years Later. Perception 25:1317–1367.

Zoccolan D (2015) Invariant visual object recognition and shape processing in rats. Behav Brain Res 285:10–33.

Zoccolan D, Di Filippo A (2018) Chapter 5 - Methodological Approaches to the Behavioural Investigation of Visual Perception in Rodents In A. Ennaceur & M. A. de Souza Silva, eds. Handbook of Behavioral Neuroscience Handbook of Object Novelty Recognition. Elsevier, p. 69–101.

Zoccolan D, Oertelt N, DiCarlo JJ, Cox DD (2009) A rodent model for the study of invariant visual object recognition. Proc Natl Acad Sci U A 106:8748–53.

Figure supplements

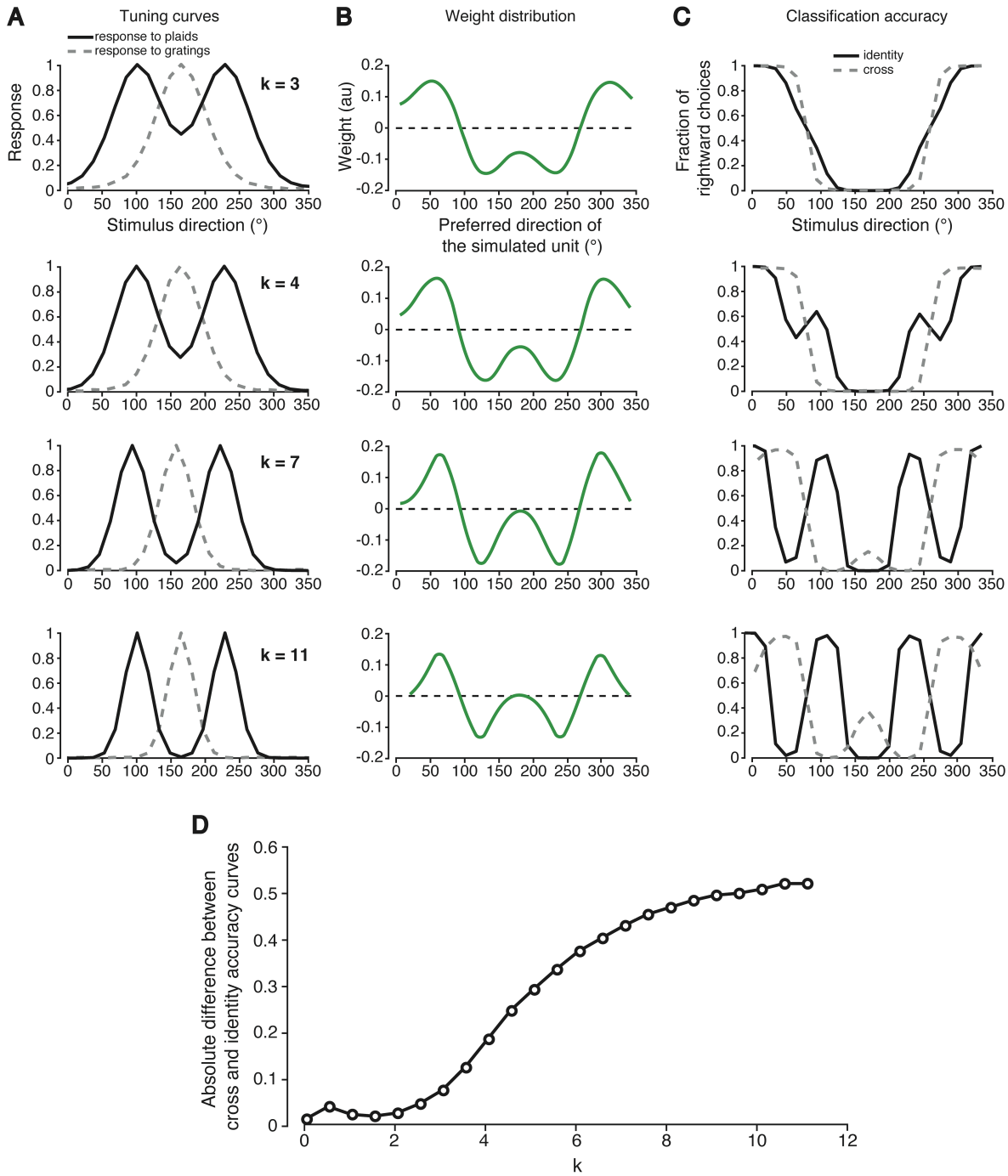

Figure 3 – figure supplement 1. Simulating the discrimination accuracy afforded by a component-based representation with different degree of direction tuning. (**A**) Example tuning curves over the direction axis, as obtained for increasingly large values of the parameter *k*, which controlled the width of the Von Mises functions used to simulate the tuning of the component cells (see main text). For each value of *k*, a population of 24 components cells was simulated, whose preferred directions homogeneously spanned the [0º 360º] range (same as in Figure 3A). The figure shows how one of such cells (the one with preferred direction = 160º) responded to drifting gratings (gray dashed curve) and plaids (black solid curve) as a function of their direction. For *k* = 7, the curves report the same values already shown in the rows of Figure 3A (top and bottom, respectively) corresponding to the

preferred direction of 160º. (**B**) Weights assigned to the 24 simulated component cells by a logistic classifier that was trained to discriminate a 0º- (rightward) from a 180º-drifting (leftward) plaid. The parameter *k* varies as indicated in A. (**C**) Fraction of times that the logistic classifier fed with the component-based representation (whose weights are shown in B) classified the test stimuli as drifting rightward (i.e., at 0º). The test stimuli were either plaids (solid black curve) or gratings (dashed gray curve) spanning the whole [0º 360º] range of directions. The parameter *k* varies as indicated in A. (**D**) Absolute difference between the pairs of curves shown in C for plaid and gratings (averaged across all tested directions) as a function of the parameter *k*.